Supporting Information for

Multidimensional MAS NMR Spectroscopy for Site-Resolved Measurement of Proton Chemical Shift Anisotropy in Biological Solids

Guangjin Hou[1,2,$], Sivakumar Paramasivam[1,$], Si Yan[1], Tatyana Polenova[1,2]*, and Alexander J. Vega[1,*]

[1]*Department of Chemistry and Biochemistry, University of Delaware, Newark, DE 19716;*
[2]*Pittsburgh Center for HIV Protein Interactions, University of Pittsburgh School of Medicine, Pittsburgh, PA 15261, United States*

AUTHOR EMAIL ADDRESS: hou@udel.edu, siva@udel.edu, syan@udel.edu, tpolenov@udel.edu, lexvega@comcast.net

[$] These authors contributed equally to this publication.

*Corresponding authors: Alexander J. Vega, University of Delaware, Department of Chemistry and Biochemistry, email: lexvega@comcast.net; Phone (302) 831-8624; Tatyana Polenova, University of Delaware, Department of Chemistry and Biochemistry; email: tpolenov@udel.edu; Phone (302) 831-1968;

MULTI-PROTON SPECTRA

For the simulation of $R12_1^4$ spectra including the effect of extra nearby protons we chose the coordinates of the $C_\alpha H$ proton and one of the $C_\beta H_2$ protons determined by Rienstra et al. for the Leu residue in *f*-MLF-OH (with the exception that we took 1.054 Å for the NH distance instead of the reported 0.98 Å in order to reproduce the DCC of 10.4 kHz used in the other simulations).[1] In addition, we added the $C_\alpha H(i-1)$ proton of the preceding Met amino acid with modified torsion angles such that it reflects the characteristic backbone structure in a β-sheet, which has this proton at a particularly short distance from the amide group under consideration. The molecular structure was transformed to a coordinate system with its *z* axis along NH and its *y* axis in the peptide plane, leading to the atomic coordinates listed in Table S1. In addition to the polar angles θ, ϕ defining the NH direction in the CSA frame of the amide proton, a third Euler angle for the orientation of the peptide plane with respect to the CSA needed to be specified. We chose the Euler angles such that the CSA tensor orientation had its *Y* axis parallel to the molecular *y* axis and its *Z* axis making a small angle θ with the NH bond, in close agreement with the conventional model depicted in Fig. 1(a). CSA tensor components that are typical for aliphatic protons[2] were assigned to the three extra protons, i. e., axially symmetric tensors with $\delta_{zz} - \delta_{iso} = 6$ ppm aligned parallel to their CH vectors. We also performed simulations including the two Hβ protons with no significant effects on the spectra (not shown).

Table S1. Atomic coordinates (in Å) in a peptide structure and their distances *d* to the amide H and N atoms based on results reported by Rienstra et al.[3] and used for the simulation of the multinuclear $R12_1^4$ spectra shown in Figure 3.

	x	*y*	*z*	d_H	d_N
H	0.000	0.000	1.045	0	1.045
N	0.000	0.000	0.000	1.045	0
Hα	0.371	-1.136	-1.688	2.991	2.068
Hβ	0.280	-2.488	1.018	2.504	2.703
Hα (*i* – 1)	-0.101	-2.087	1.293	2.103	2.457

Table S2. Spin-interaction parameters used for the simulation of the four-proton spectra shown in Figure 3 and the parameters obtained by triple curve fitting using full Hamiltonian $^{1}H^{15}N$ Hamiltonian or average Hamiltonian. The atomic coordinates of N and H atoms are given in Table S1.

	$\delta_{XX} - \delta_{iso}$	$\delta_{YY} - \delta_{iso}$	$\delta_{ZZ} - \delta_{iso}$	span	DCC	θ
NH_4 simulated	5.5	-1.5	-4.0	9.5	10.0	10°
full NH Hamilt. fit	6.1	-1.7	-4.4	10.4	10.1	18°
average Hamilt. fit	6.1	-2.0	-4.1	10.3	10.0	13°
NH_4 simulated	5.0	1.0	-6.0	11.0	10.0	10°
full NH Hamilt. fit	6.0	-0.1	-5.9	11.9	9.8	9°
average Hamilt. fit	6.2	0.0	-6.2	12.4	10.0	9°
NH_4 simulated	8.0	-1.0	-7.0	15.0	10.0	5°
full NH Hamilt. fit	8.3	-1.4	-6.9	15.2	9.7	5°
average Hamilt. fit	8.5	-1.4	-7.1	15.5	9.9	0°
NH_4 simulated	8.0	-1.0	-7.0	15.0	10.0	20°
full NH Hamilt. fit	8.3	-1.4	-6.9	15.1	9.7	21°
average Hamilt. fit	8.5	-1.6	-6.9	15.3	10.0	20°
NH_4 simulated	8.0	2.0	-10.0	18.0	10.0	5°
full NH Hamilt. fit	8.4	1.8	-10.2	18.6	9.6	6°
average Hamilt. fit	8.4	2.3	-10.7	19.2	9.9	7°
NH_4 simulated	8.0	2.0	-10.0	18.0	10.0	20°
full NH Hamilt. fit	7.8	2.4	-10.2	18.1	9.6	22°
average Hamilt. fit	7.7	2.7	-10.4	18.0	9.9	21°

Table S3. Summary of the first- and second-order terms present in the Hamiltonians of four R*N*-symmetry sequences suitable for recoupling of ^{1}H chemical shift anisotropy.

<table>
<tr><th>Sequence</th><th>First-order terms</th><th>Second-order terms</th></tr>
<tr><td>$R18_2^5$</td><td>
<table>
<tr><th>DD</th><th>CSA</th><th>isoCS</th><th>rf</th><th>J</th></tr>
<tr><td>0</td><td>2</td><td>0</td><td>0</td><td>1</td></tr>
</table>
</td><td>
<table>
<tr><th></th><th>DD</th><th>CSA</th><th>isoCS</th><th>rf</th><th>J</th></tr>
<tr><td>DD</td><td>16</td><td>38</td><td>6</td><td>0</td><td>0</td></tr>
<tr><td>CSA</td><td>38</td><td>36</td><td>4</td><td>4</td><td>12</td></tr>
<tr><td>isoCS</td><td>6</td><td>4</td><td>2</td><td>0</td><td>3</td></tr>
<tr><td>rf</td><td>0</td><td>4</td><td>0</td><td>2</td><td>2</td></tr>
<tr><td>J</td><td>0</td><td>12</td><td>3</td><td>2</td><td>0</td></tr>
</table>
</td></tr>
<tr><td>$R18_1^7$</td><td>
<table>
<tr><th>DD</th><th>CSA</th><th>isoCS</th><th>rf</th><th>J</th></tr>
<tr><td>0</td><td>2</td><td>0</td><td>0</td><td>1</td></tr>
</table>
</td><td>
<table>
<tr><th></th><th>DD</th><th>CSA</th><th>isoCS</th><th>rf</th><th>J</th></tr>
<tr><td>DD</td><td>16</td><td>38</td><td>6</td><td>0</td><td>0</td></tr>
<tr><td>CSA</td><td>38</td><td>36</td><td>4</td><td>4</td><td>12</td></tr>
<tr><td>isoCS</td><td>6</td><td>4</td><td>2</td><td>0</td><td>3</td></tr>
<tr><td>rf</td><td>0</td><td>4</td><td>0</td><td>2</td><td>2</td></tr>
<tr><td>J</td><td>0</td><td>12</td><td>3</td><td>2</td><td>0</td></tr>
</table>
</td></tr>
<tr><td>$R12_1^4$</td><td>
<table>
<tr><th>DD</th><th>CSA</th><th>isoCS</th><th>rf</th><th>J</th></tr>
<tr><td>0</td><td>2</td><td>0</td><td>0</td><td>1</td></tr>
</table>
</td><td>
<table>
<tr><th></th><th>DD</th><th>CSA</th><th>isoCS</th><th>rf</th><th>J</th></tr>
<tr><td>DD</td><td>24</td><td>42</td><td>10</td><td>0</td><td>0</td></tr>
<tr><td>CSA</td><td>42</td><td>40</td><td>4</td><td>4</td><td>12</td></tr>
<tr><td>isoCS</td><td>10</td><td>4</td><td>2</td><td>0</td><td>3</td></tr>
<tr><td>rf</td><td>0</td><td>4</td><td>0</td><td>2</td><td>2</td></tr>
<tr><td>J</td><td>0</td><td>12</td><td>3</td><td>2</td><td>0</td></tr>
</table>
</td></tr>
<tr><td>$R26_2^9$</td><td>
<table>
<tr><th>DD</th><th>CSA</th><th>isoCS</th><th>rf</th><th>J</th></tr>
<tr><td>0</td><td>2</td><td>0</td><td>0</td><td>1</td></tr>
</table>
</td><td>
<table>
<tr><th></th><th>DD</th><th>CSA</th><th>isoCS</th><th>rf</th><th>J</th></tr>
<tr><td>DD</td><td>16</td><td>38</td><td>6</td><td>0</td><td>0</td></tr>
<tr><td>CSA</td><td>38</td><td>36</td><td>4</td><td>4</td><td>12</td></tr>
<tr><td>isoCS</td><td>6</td><td>4</td><td>2</td><td>0</td><td>3</td></tr>
<tr><td>rf</td><td>0</td><td>4</td><td>0</td><td>2</td><td>2</td></tr>
<tr><td>J</td><td>0</td><td>12</td><td>3</td><td>2</td><td>0</td></tr>
</table>
</td></tr>
</table>

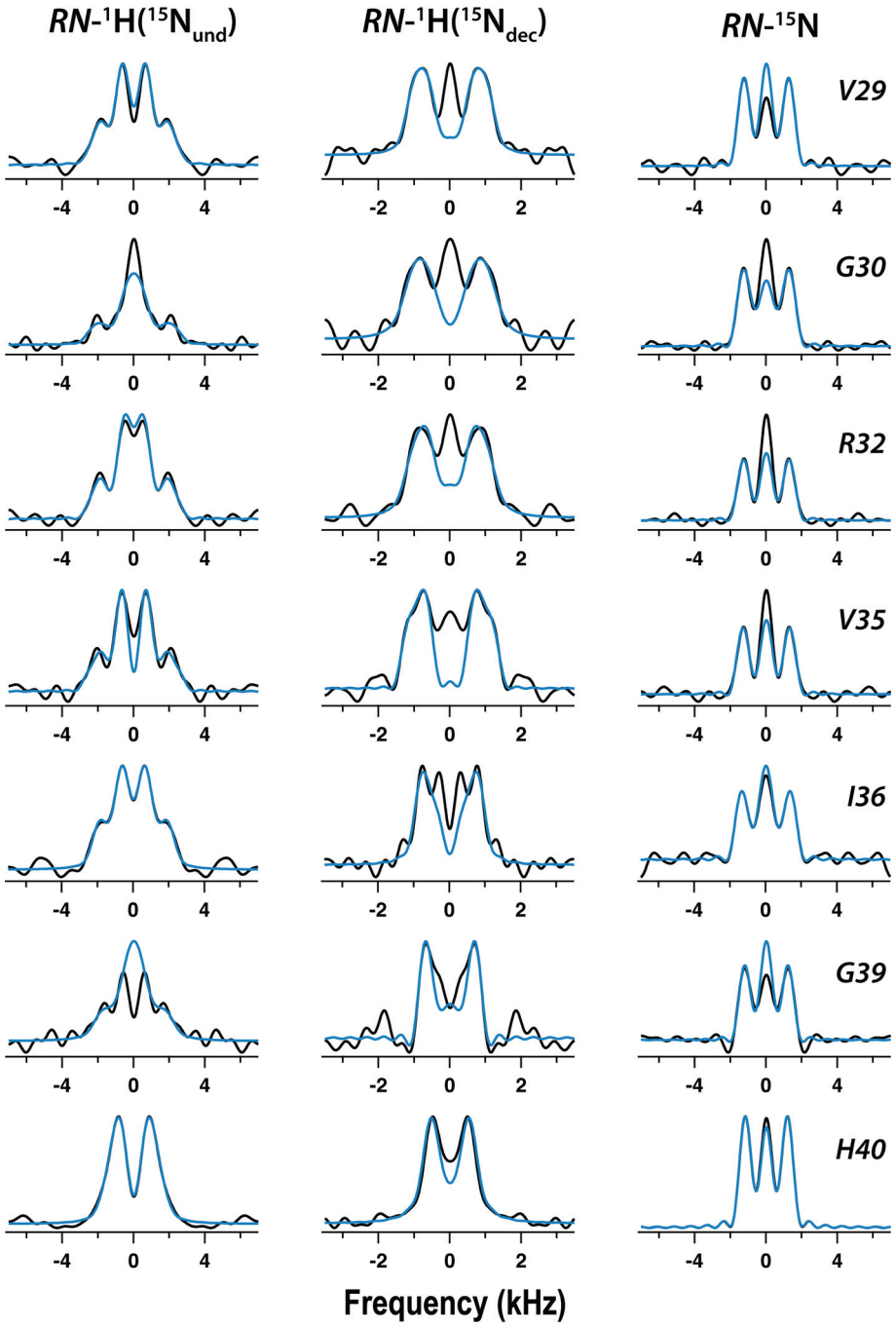

Figure S1. Experimental (black) and best-fit simulated with full Hamiltonian (blue) $R12_1^4$-symmetry based *RN*-^{1}H($^{15}N_{und}$), *RN*-^{1}H($^{15}N_{dec}$), and *RN*-^{15}N lineshapes of residues V29 – H40 of U-^{13}C,^{15}N-CAP-Gly domain of mammalian dynactin.

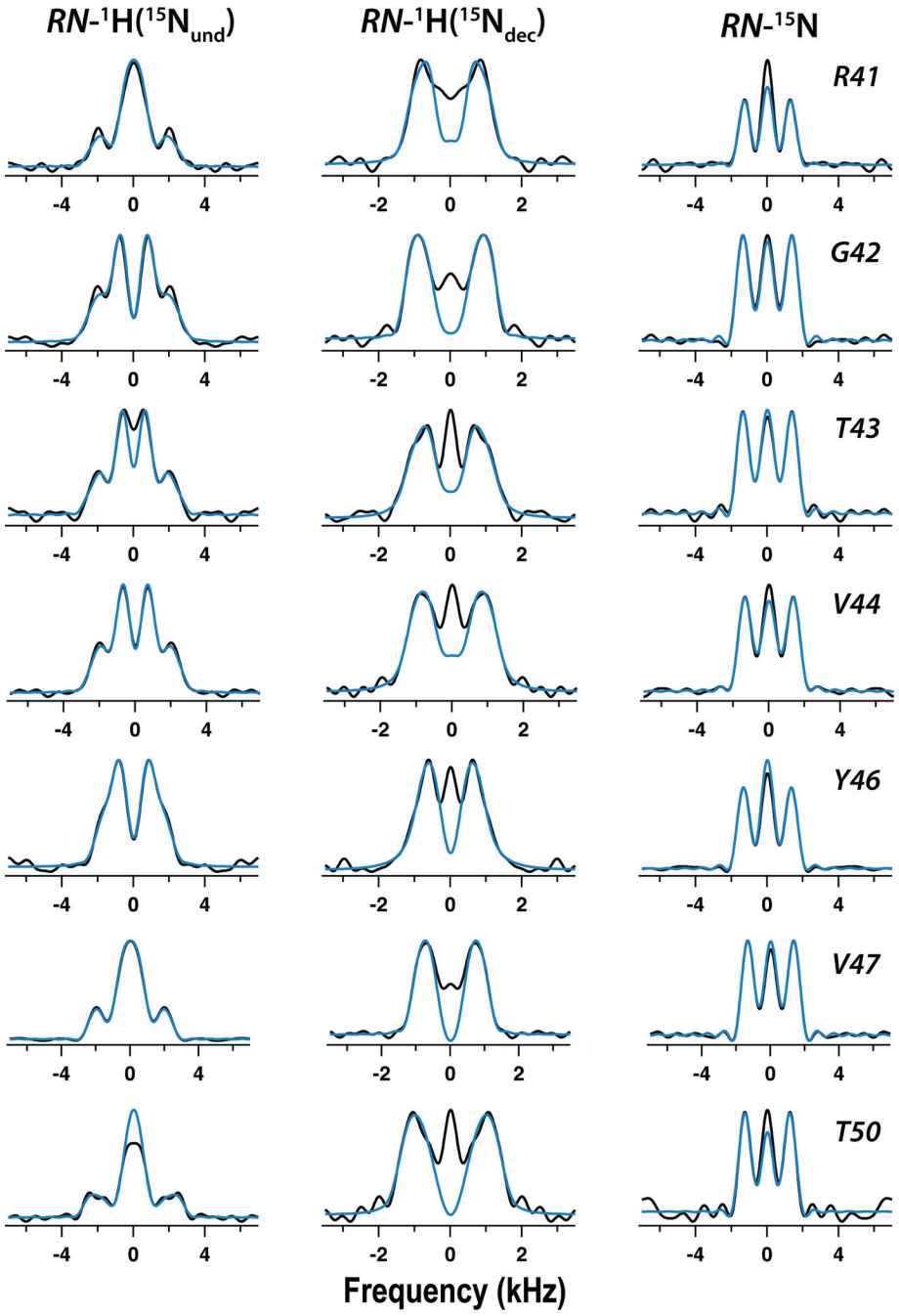

Figure S2. Experimental (black) and best-fit simulated with full Hamiltonian (blue) $R12_1^4$-symmetry based *RN*-^{1}H(^{15}N$_{und}$), *RN*-^{1}H(^{15}N$_{dec}$), and *RN*-^{15}N lineshapes of residues R41 – T50 of U-^{13}C,^{15}N-CAP-Gly domain of mammalian dynactin.

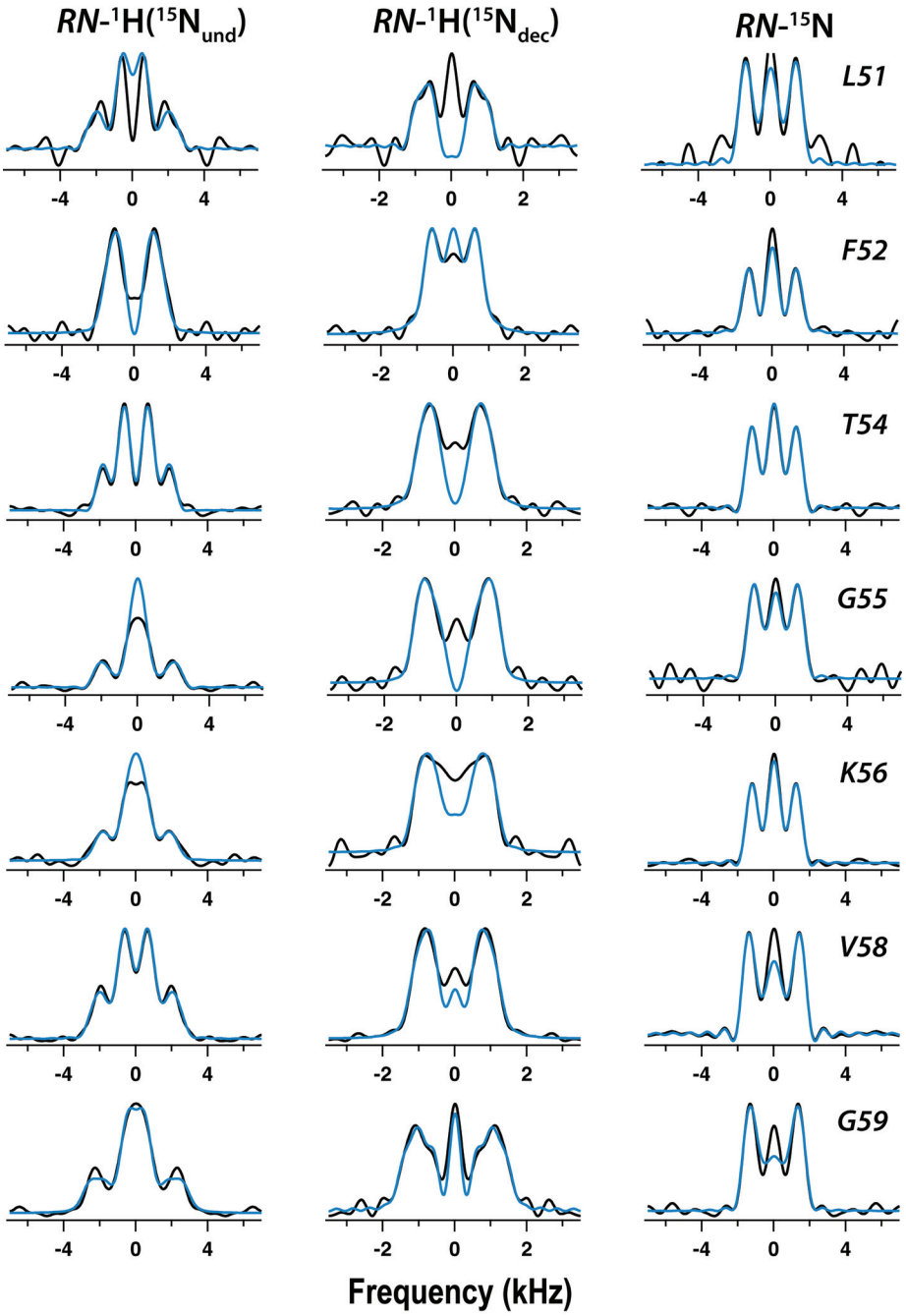

Figure S3. Experimental (black) and best-fit simulated with full Hamiltonian (blue) $R12_1^4$-symmetry based *RN*-^{1}H(^{15}N$_{und}$), *RN*-^{1}H(^{15}N$_{dec}$), and *RN*-^{15}N lineshapes of residues L51 – G59 of U-^{13}C,^{15}N-CAP-Gly domain of mammalian dynactin.

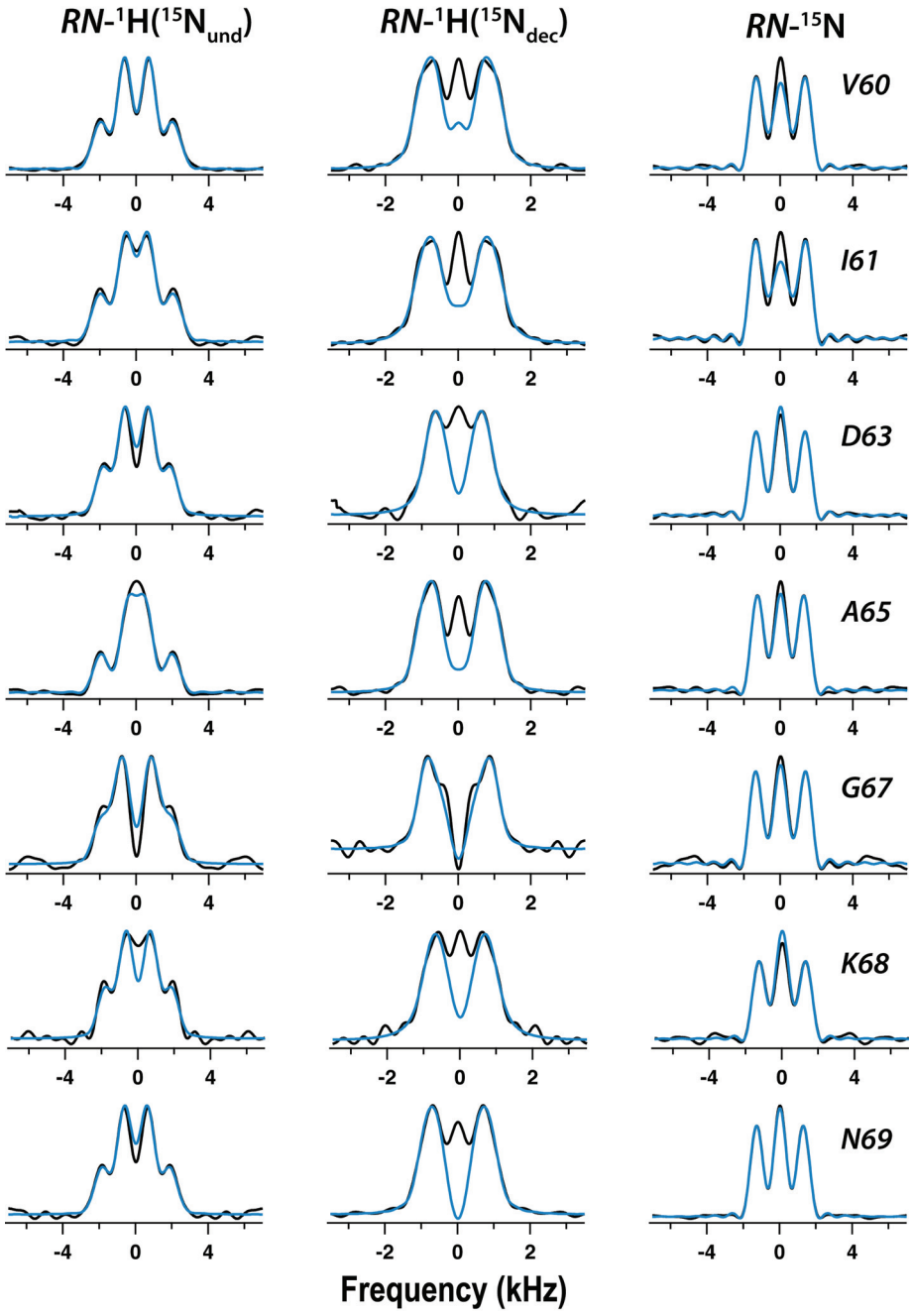

Figure S4. Experimental (black) and best-fit simulated with full Hamiltonian (blue) $R12_1^4$-symmetry based *RN*-^{1}H(^{15}N$_{und}$), *RN*-^{1}H(^{15}N$_{dec}$), and *RN*-^{15}N lineshapes of residues V60 – N60 of U-^{13}C,^{15}N-CAP-Gly domain of mammalian dynactin.

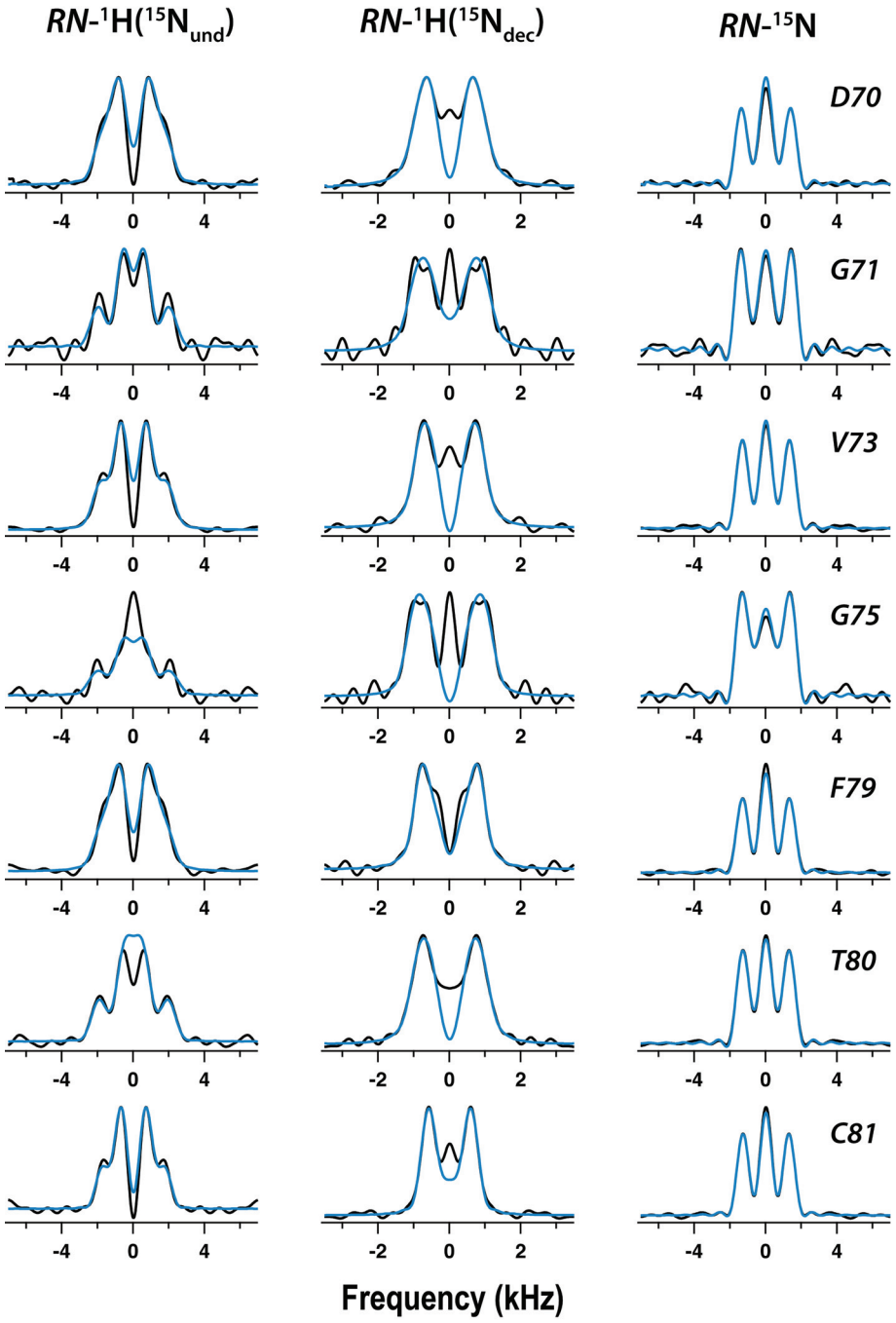

Figure S5. Experimental (black) and best-fit simulated with full Hamiltonian (blue) $R12_1^4$-symmetry based *RN*-^{1}H($^{15}N_{und}$), *RN*-^{1}H($^{15}N_{dec}$), and *RN*-^{15}N lineshapes of residues D70 – C81 of U-^{13}C,^{15}N-CAP-Gly domain of mammalian dynactin.

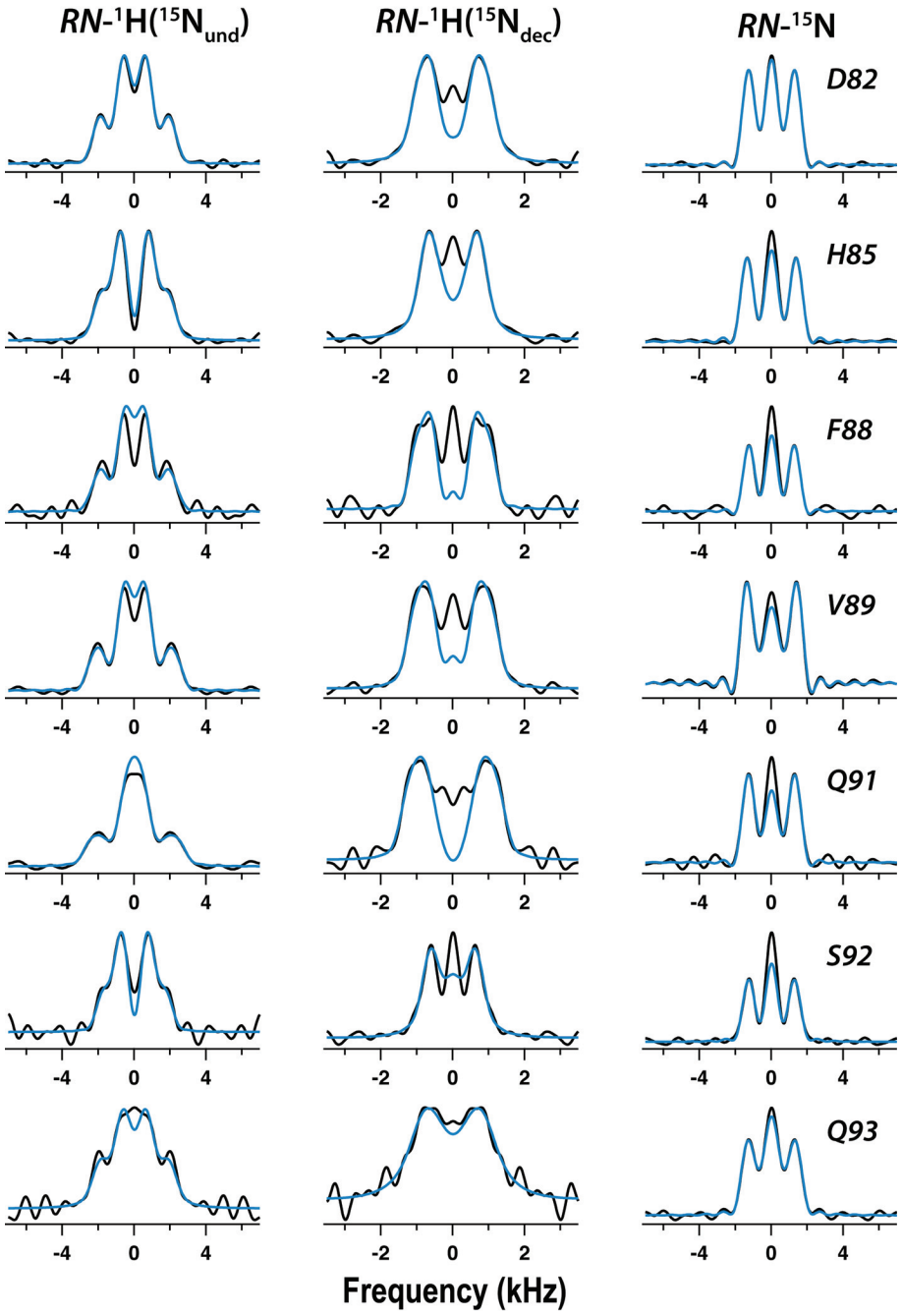

Figure S6. Experimental (black) and best-fit simulated with full Hamiltonian (blue) $R12_1^4$-symmetry based *RN*-^{1}H(^{15}N$_{und}$), *RN*-^{1}H(^{15}N$_{dec}$), and *RN*-^{15}N lineshapes of residues D82 – Q93 of U-^{13}C,^{15}N-CAP-Gly domain of mammalian dynactin.

References

(1) Rienstra, C. M.; Tucker-Kellogg, L.; Jaroniec, C. P.; Hohwy, M.; Reif, B.; McMahon, M. T.; Tidor, B.; Lozano-Perez, T.; Griffin, R. G. *Proc. Natl. Acad. Sci. USA* **2002**, *99*, 10260-10265.

(2) Duncan, T. M. *A Compilation of Chemical Shift Anisotropies*; Farragut Press, Chicago, United States, **1990**.

(3) Rienstra, C. M.; Hohwy, M.; Mueller, L. J.; Jaroniec, C. P.; Reif, B.; Griffin, R. G. *J. Am. Chem. Soc.* **2002**, *124*, 11908-11922.